PCCP

PAPER

View Article Online
View Journal | View Issue

Cite this: *Phys. Chem. Chem. Phys.*, 2026, **28**, 2608

Turn-off fluorescence sensing of benzenediols *via* guest-induced π-conjugation switching in bisimidazole-based hydrindacene allosteric receptors

Takayuki Kataoka, Yoshitaka Tsuchido and Hidetoshi Kawai *

Received 20th October 2025,
Accepted 30th December 2025

DOI: 10.1039/d5cp04027b

rsc.li/pccp

Fluorescent bisimidazole-based hydrindacene allosteric receptors **1a–c** and **2** were synthesized for non-linear ON/OFF sensing of benzenediols. By tuning their D–π–D conjugation through substituent modification, these receptors were designed to function as turn-off fluorescent sensors based on the cleavage of their π-conjugation accompanied by binding with benzenediols. The cooperative allosteric binding demonstrated selective and efficient nonlinear quenching toward orcinol.

Introduction

Imidazole is a five-membered heteroaromatic ring with two electronically distinct nitrogen atoms, an electron donor and an electron acceptor.[1,2] This dual electronic nature allows the electronic behavior of imidazole to be tuned based on the substituents on the ring. Depending on whether an electron-withdrawing/neutral or electron-donating group is attached at the C2-position, imidazole can act as an electron-donating[3–5] or electron-accepting unit,[6–8] respectively. Due to these unique electronic characteristics, imidazole serves as a versatile building block for constructing chromophores,[9] fluorescent materials with intramolecular charge transfer (ICT)[10,11] or excited state intramolecular proton transfer (ESIPT) properties,[12,13] and as ancillary ligands for phosphorescent materials.[14,15] Particularly, these luminescent properties have also been applied to the design of chemical sensors capable of selectively detecting specific metal[4,5,16–19] and non-metal ions,[20–24] and chemical species with particular functional groups.[25–30] Although such fluorescent sensors exhibit a linear response proportional to guest concentration and are suitable for quantitative analysis, they rely on an intensity change associated with 1 : 1 complexation as a threshold, which presents limitations in improving selectivity. To overcome this limitation and enhance selectivity, approaches based on positive homotropic allosteric binding have recently garnered attention.[31–34] The sigmoidal nonlinear response, in which binding of a guest molecule strengthens further binding of the same guest, is expected to enable improved sensitivity and selectivity.

Recently, we developed hydrindacene-based allosteric receptors with benzimidazole units that form 1 : 2 host–guest complexes with benzenediols (Scheme 1a).[35] These bisimidazole D–π–D systems function as highly π-conjugated chromophores.[36–38] In our system, guest binding induces a conformational twist in the benzimidazole units, which disrupts their π-conjugation and changes their spectroscopic properties. Unlike typical fluorescent sensors that show a linear response from 1 : 1 binding, our allosteric system exhibits the desired nonlinear response,[31] enabling sharp ON/OFF switching once a concentration threshold is exceeded. This makes it a promising candidate for application in biosensing

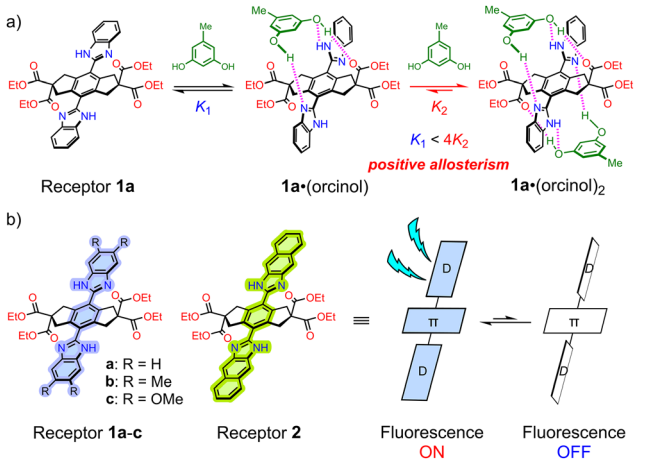

Scheme 1 (a) Allosteric binding of the bisimidazole-based hydrindacene receptor **1a** with orcinol.[35] (b) Fluorescent receptors **1a–c** (with benzimidazole units) and receptor **2** (with naphthoimidazole units), along with the proposed fluorescence quenching mechanism *via* D–π–D twisting (this work).

Department of Chemistry, Faculty of Science, Tokyo University of Science, 1-3 Kagurazaka, Shinjuku-ku, Tokyo 162-8601, Japan. E-mail: kawaih@rs.tus.ac.jp

and environmental monitoring, where a clear threshold and enhanced guest selectivity are desired.[32–34]

Herein, we investigate how substituents and π-conjugation extension influence the fluorescence sensing behavior of bisimidazole-based hydrindacene allosteric receptors through selective and cooperative guest binding (Scheme 1b). We synthesized a series of receptors, bisbenzimidazole **1a–c** and bisnaphthoimidazole **2**, whose emission colors were precisely tuned. Their fluorescence was efficiently quenched upon addition of benzenediols. Notably, orcinol induced nonlinear fluorescence quenching with increasing guest concentration due to allosteric 1 : 2 complexation. Our research demonstrates that this system functions as a turn-off supramolecular fluorescent sensor that exhibits enhanced guest selectivity and distinct emission changes in the visible-light region, unlike conventional benzenediol sensors.[39–41]

Results and discussion

Preparation of bisimidazole-based hydrindacene receptors

Receptors **1a** and **1b** were prepared as shown in Scheme 2, following our previously reported procedure.[35] The diiode compound **3** was first converted to the dicyano compound by cyanation with CuCN. Subsequent hydrolysis with hydrogen peroxide afforded the diamide compound **4**. The amide groups of **4** were then converted to the imidate intermediate **5** using Meerwein reagent, followed by condensation with 1,2-phenylenediamine or 4,5-dimethyl-1,2-phenylenediamine to give receptor **1a** and receptor **1b**, respectively.

Receptors **1c** and **2** were also prepared from **3**. The diiodo compound **3** was converted to the diformyl compound **6** using the Bouveault aldehyde synthesis.[42] The subsequent condensation of **6** with 4,5-dimethoxy-1,2-phenylenediamine or 2,3-diaminonaphthalene in nitrobenzene/AcOH[43] afforded receptor **1c** and receptor **2**, respectively.

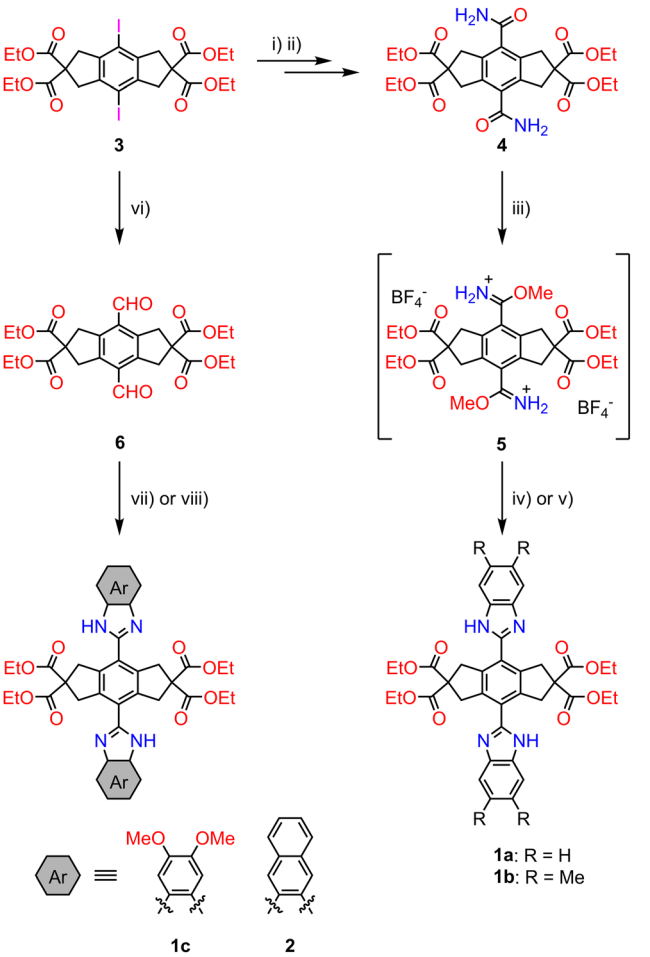

Scheme 2 Synthesis of receptors **1a–1c** and **2**. Reagents and conditions: (i) CuCN, DMF, 150 °C, 16 h, 92%; (ii) H_2O_2 aq., K_2CO_3, acetone/DMSO, r.t., 3 d, 89%; (iii) $Me_3O^+ \cdot BF_4^-$, CH_2Cl_2, reflux, 2 d; (iv) 1,2-phenylenediamine, EtOH, reflux, 3 d, 2 steps 8%; (v) 4,5-dimethyl-1,2-phenylenediamine, EtOH, reflux, 3 d, 2 steps 7%; (vi) ^{i}PrMgCl·LiCl, DMF, THF, −78 °C to r.t., 19 h, 78%; (vii) 4,5-dimethoxy-1,2-phenylenediamine, nitrobenzene/AcOH, 60 °C, 21 h, 38%; (viii) 2,3-diaminonaphthalene, nitrobenzene/AcOH, 60 °C, 2 d, 50%.

X-ray structures of guest-free receptors

The structures of bisbenzimidazole receptor **1a**[35] and bisnaphthoimidazole receptor **2** were elucidated by single-crystal X-ray structural analysis (Fig. 1). Both crystal structures of **1a** and **2** include two molecules of methanol used as the recrystallization solvent with hydrogen bond formation between the amidine unit. The amidine units and phenylene ring of the hydrindacene framework were slightly tilted (34.0° in **1a** and 28.0° in **2**, respectively).

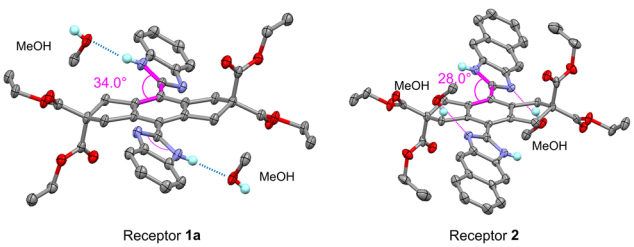

Fig. 1 X-ray crystal structures of receptors **1a** and **2**. Amidine N forms hydrogen bonds with the solvent methanol. Hydrogen atoms of C–H are omitted for clarity.

Allosteric binding of bisimidazole-based receptors toward benzenediols

First, to evaluate the guest-selective allosteric binding ability of the receptors—an essential step for demonstrating the nonlinear fluorescence quenching causing by D–π–D conjugation cleavage upon allosteric guest binding—we investigated the complexation behavior of receptor **1a** with three representative guests (orcinol, catechol, and phenol) by ^{1}H NMR spectroscopy in $CDCl_3$ (Fig. 2). Upon addition of orcinol, the NH proton signal of the benzimidazole unit shifted downfield to 10.81 from 9.51 ppm ($\Delta\delta$ = +1.30 ppm), and the methylene proton signal of the five-membered ring (H_a) shifted upfield to 3.15 from 3.86 ppm ($\Delta\delta$ = −0.71 ppm). This suggests that **1a** forms hydrogen bonds with orcinol, which is accompanied by

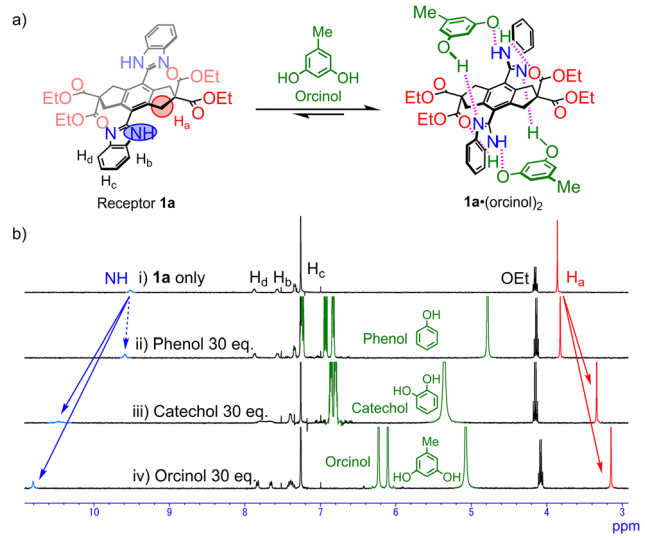

Fig. 2 (a) Complexation of receptor **1a** with orcinol. (b) ^{1}H NMR spectra of (i) **1a** only, (ii) **1a** with 30 eq. of phenol, (iii) **1a** with 30 eq. of catechol, (iv) **1a** with 30 eq. of orcinol in $CDCl_3$.

shielding on the methylene protons by the benzene ring of the guest. The addition of catechol also caused a downfield shift of the NH proton ($\Delta\delta$ = +0.95 ppm) and an upfield shift of H_a ($\Delta\delta$ = −0.52 ppm), indicating a weaker guest binding than that with orcinol. In contrast, the addition of phenol induced only minor shifts in the NH proton ($\Delta\delta$ = +0.08 ppm) and H_a ($\Delta\delta$ = −0.04 ppm). These results indicate that, similar to the previously reported hydrindacenediamide receptor,[44] the bisimidazole receptors also selectively bind to benzenediols rather than phenol through cooperative hydrogen-bond formation based on allosteric binding.[45] The NMR titration profiles for orcinol and catechol were in good agreement with a 1 : 2 binding model as confirmed by curve fitting.[46] The macroscopic binding constants, K_1, K_2, and cooperative factor, α (= $4K_2/K_1$), were estimated.[47] The values for orcinol were K_1 = 70 ± 9.1 M^{-1}, K_2 = 3560 ± 460 M^{-1}, and α = 210, while for catechol they were K_1 = 74 ± 14 M^{-1}, K_2 = 136 ± 23 M^{-1}, and α = 7.3. Both binding strength and cooperativity with orcinol were significantly greater than with catechol.

Spectroscopic properties of bisimidazole-based receptors

Next, the spectroscopic properties of the receptors were examined in CH_2Cl_2 and DMSO (Fig. 3 and Table 1; additional spectra in acetone and MeCN are provided in the SI: Fig. S11, S13, S15 and S17). While benzimidazole (**BZI**) itself was non-emissive, all bisimidazole-based hydrindacene D–π–D receptors **1a–c** and **2** exhibited clear fluorescence.

The fluorescence spectra of **1a–c** correspond to the electron-donating properties of the substituents,[48] showing progressive red-shifts in the order **1a** < **1b** < **1c** (Fig. 3): receptor **1a** exhibited deep blue emission (λ_{em} = 395 nm, φ_F = 0.67 in CH_2Cl_2; λ_{em} = 395 nm, φ_F = 0.64 in DMSO); **1b** exhibited blue emission (λ_{em} = 412 nm, φ_F = 0.62 in CH_2Cl_2; λ_{em} = 412 nm, φ_F = 0.59 in DMSO); and **1c** exhibited light blue emission

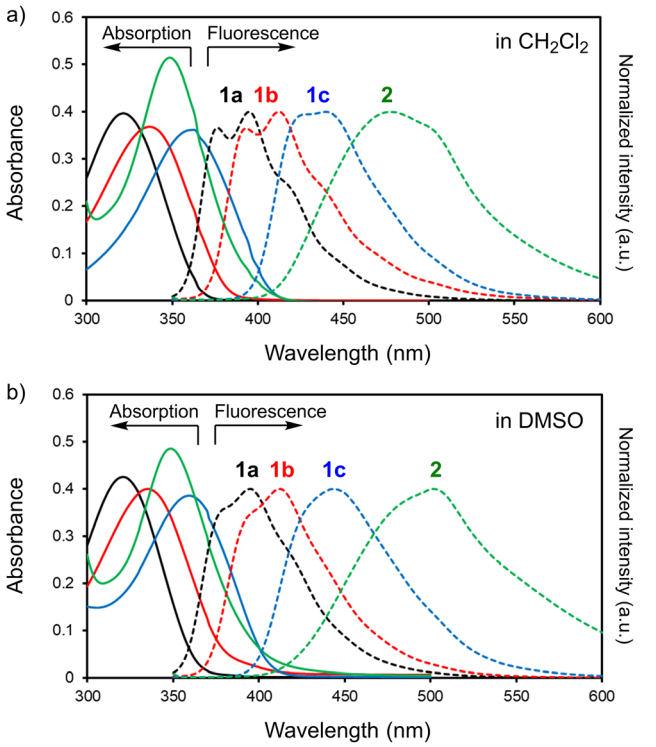

Fig. 3 UV/Vis absorption (solid lines) and fluorescence (dotted lines) spectra of receptors **1a** (black), **1b** (red), **1c** (blue), and **2** (green) in (a) CH_2Cl_2 and (b) DMSO (10 μM).

Table 1 Spectroscopic properties of **1a–c** and **2** in CH_2Cl_2 and DMSO (10 μM)

Receptor	Solvent	λ_{abs} (nm)	λ_{em} (nm)	Stokes shift (cm^{-1})	φ_F[a]
BZI	CH_2Cl_2	274	—	—	—
	DMSO	275	—	—	—
1a	CH_2Cl_2	322	395	5740	0.67
	DMSO	321	395	5840	0.64
1b	CH_2Cl_2	337	412	5400	0.62
	DMSO	335	412	5580	0.59
1c	CH_2Cl_2	363	440	4820	0.72
	DMSO	359	444	5330	0.68
2	CH_2Cl_2	349	478	7730	0.24
	DMSO	349	501	8690	0.20

[a] Fluorescence quantum yield (φ_F) was determined relative to quinine sulfate in 0.5 M H_2SO_4 (φ_F = 0.546).

(λ_{em} = 440 nm, φ_F = 0.72 in CH_2Cl_2; λ_{em} = 444 nm, φ_F = 0.68 in DMSO). The emission maxima (λ_{em}) remained nearly unchanged regardless of solvent polarity, which suggests that intramolecular charge transfer (ICT) is not a dominant feature in these systems. DFT calculations revealed that the electron-donating groups raised the HOMO energy levels while having a marginal effect on the LUMO energy levels, thereby narrowing the HOMO–LUMO energy gap (Fig. 4).

The fluorescence spectrum of receptor **2** was further red-shifted, emitting a light green fluorescence. This result is consistent with DFT calculations, showing that the naphthoimidazole units narrow the HOMO–LUMO energy gap. This is attributed to the localization of the HOMO on the

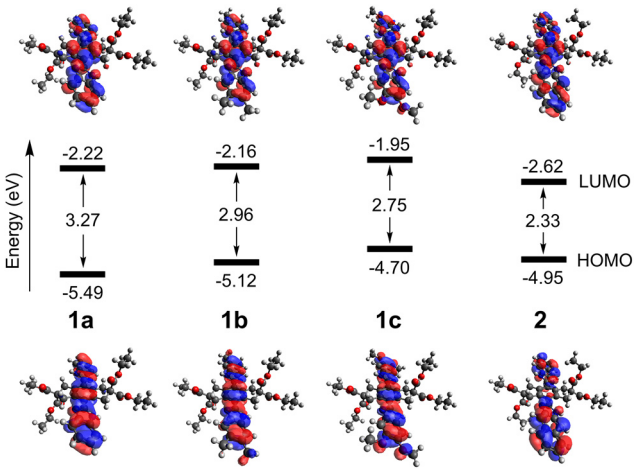

Fig. 4 HOMO and LUMO energy levels and Kohn–Sham orbitals of receptors **1a–c** and **2**, calculated at the r^2SCAN-3c/def2-mTZVPP level.

naphthoimidazole unit, which raises its energy level, whereas the LUMO is delocalized over both the naphthoimidazole and phenylene units, resulting in a lower energy level due to the extended π-conjugation. Furthermore, λ_{em} of **2** exhibited a large solvatochromic effect (λ_{em} = 478 nm, φ_F = 0.24 in CH_2Cl_2; λ_{em} = 501 nm, φ_F = 0.20 in DMSO). This large red-shift of 23 nm, with λ_{em} shifting from 478 to 501 nm, suggests the presence of intramolecular charge transfer (ICT) characteristics dependent on the solvent polarity.

Fluorescence intensity changes due to guest binding

To evaluate fluorescence changes induced by guest binding and protonation, the spectroscopic properties of each receptor in CH_2Cl_2 were examined (Fig. 5 and Table 2).

First, upon addition of phenol, only a slight blue-shift in the absorption maxima (λ_{abs}) was observed (**1a:** λ_{abs} = 322 to 318 nm; **1b:** λ_{abs} = 337 to 331 nm; **1c:** λ_{abs} = 363 to 357 nm; **2:** λ_{abs} = 349 to 346 nm). Although a minor decrease in relative fluorescence intensity (RFI: 0.58–0.78) was noted, no significant quenching was observed. This result indicates that simple

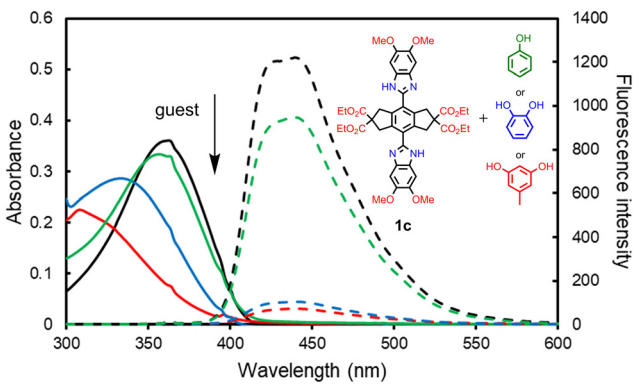

Fig. 5 UV-Vis absorption (solid lines) and fluorescence (dotted lines) spectra of receptor **1c** (black), **1c** with orcinol (red), **1c** with catechol (blue), and **1c** with phenol (green) in CH_2Cl_2 (**1c**: 10 μM; orcinol, catechol, and phenol: 30 mM).

Table 2 Spectroscopic properties of receptors **1a–c** and **2** upon adding benzenediols and phenol in CH_2Cl_2 (receptors: 10 μM; orcinol, catechol, and phenol: 30 mM)

Receptor	λ_{abs} (nm)	λ_{em} (nm)	φ_F[a]	RFI
1a	322	395	0.67	1
1a + orcinol	—	395	0.047	0.020
1a + catechol	—	395	0.057	0.047
1a + phenol	318	395	0.38	0.58
1a + TFA	303	401	0.52	—
1b	337	412	0.62	1
1b + orcinol	—	412	0.049	0.030
1b + catechol	—	412	0.047	0.054
1b + phenol	331	412	0.38	0.75
1b + TFA	316	426	0.55	—
1c	363	440	0.72	1
1c + orcinol	308	440	0.16	0.060
1c + catechol	333	441	0.10	0.085
1c + phenol	357	439	0.60	0.78
1c + TFA	345	503	0.63	—
2	349	476	0.24	1
2 + orcinol	330	479	0.025	0.046
2 + catechol	335	482	0.027	0.081
2 + phenol	346	479	0.17	0.65
2 + TFA	337	580	0.006	—

[a] Fluorescence quantum yield (φ_F) was determined relative to quinine sulfate in 0.5 M H_2SO_4 (φ_F = 0.546).

phenol does not cause either fluorescence quenching or a red-shift in the emission maxima (λ_{em}) that would be induced by protonation of the amidine units or ESIPT-like proton transfer in the excited state. The addition of TFA led to protonation of the imidazole units, resulting in a blue-shift in λ_{abs} and a red-shift in λ_{em} (**1a:** λ_{abs} = 322 to 303 nm, λ_{em} = 395 to 401 nm; **1b:** λ_{abs} = 337 to 316 nm, λ_{em} = 412 to 426 nm; **1c:** λ_{abs} = 363 to 345 nm, λ_{em} = 440 to 503 nm; **2:** λ_{abs} = 349 to 337 nm, λ_{em} = 476 to 580 nm). In this case as well, no significant quenching was observed, except for receptor **2**.[49]

Upon addition of benzenediols, all receptors exhibited a blue-shift in λ_{abs} (**1c:** λ_{abs} = 363 to 308 nm; **2:** λ_{abs} = 349 to 330 nm)[50] and a significant quenching of fluorescence (RFI: 0.020–0.085) (Fig. 6 and 7). We attribute these blue-shifts to the change in π-conjugation from an extended imidazole–phenylene–imidazole D–π–D system to imidazole units with reduced conjugation efficiency,[35] in which this D–π–D twisting raises the LUMO energy level and lowers HOMO energy level of the receptor (Fig. S29). In addition, this change promotes a shift of the HOMO toward the guest molecule, facilitating CT excited states from the guest to the twisted receptor (Fig. S30), resulting in the loss of the fluorescence property as a π-extended D–π–D chromophore in its initial state.[51]

Given that this quenching is induced by allosteric binding, it is expected to exhibit the desired nonlinear response. Therefore, the changes in fluorescence intensity of **1a** were further investigated upon the sequential addition of benzenediols (Fig. 8). The Stern–Volmer plot, constructed by plotting I_0/I against guest concentration, exhibited a curved and nonlinearly increasing profile (Fig. 8b).[52] This confirmed a nonlinear

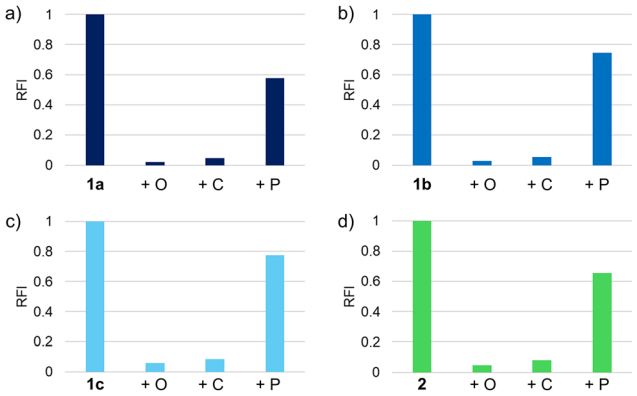

Fig. 6 Relative fluorescence intensities of receptors (a) **1a**, (b) **1b**, (c) **1c**, (d) **2** upon adding orcinol (O), catechol (C), and phenol (P) in CH_2Cl_2 (receptors: 10 μM; orcinol, catechol, and phenol: 30 mM).

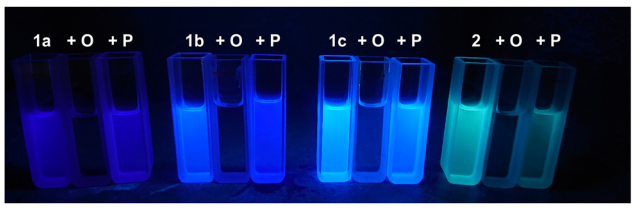

Fig. 7 Photographs showing the fluorescence color of receptors **1a–c** and **2** upon adding orcinol (O) and phenol (P) under UV light (365 nm) in CH_2Cl_2 (receptors: 10 μM; orcinol, catechol, and phenol: 30 mM).

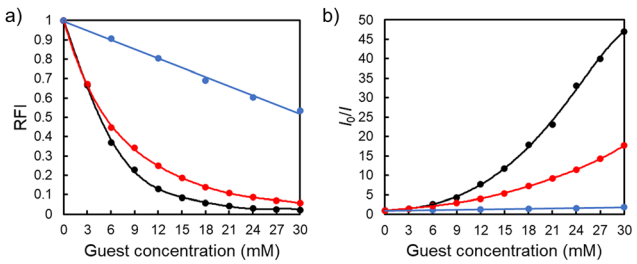

Fig. 8 (a) The decrease in relative fluorescence intensity with respect to guest concentration. (b) Stern–Volmer plots of receptor **1a** in the presence of orcinol (black), catechol (red), and phenol (blue).

response based on allosteric binding, in which fluorescence quenching is accelerated with increasing guest concentration.

The limits of detection (LODs) for orcinol, catechol, and phenol were estimated 21, 34, and 362 μM, respectively, using the empirical equation LOD = $3\sigma/K_{SV}$ (Fig. S20).[27] In addition, the selectivity ratios for orcinol/catechol and orcinol/phenol were amplified to 3 and 50, respectively, at higher concentrations (Fig. S21 and S22). These remarkable results, which are attributed to the nonlinear behavior based on positive allosteric binding, demonstrate the successful integration of the allosteric effect for highly selective fluorescence quenching-based sensing.

Furthermore, investigation of the quenching behavior of the receptor based on the Stern–Volmer plot and fluorescence lifetime measurements (Fig. S23 and S24) revealed that the quenching process is predominantly static quenching, and that non-binding guest molecules have little influence on the emission of the receptors (Table S2).[53]

These results collectively indicate that fluorescence quenching occurs specifically with benzenediols capable of allosteric binding, thereby demonstrating excellent guest selectivity. Furthermore, they suggest that these receptors have the potential to function as highly selective "turn-off" fluorescent sensors with nonlinear response characteristics, particularly toward 1,3-benzenediol derivatives.

Conclusions

In conclusion, we successfully synthesized a series of fluorescent bisimidazole-based hydrindacene allosteric receptors. These receptors demonstrated high fluorescence quantum yields and tunable emission colors, ranging from deep blue to light green, which can be modulated by the electron-donating nature of the substituents and the extent of π-conjugation. We found that these receptors underwent selective 1 : 2 allosteric binding with benzenediols, inducing disruption of the extended π-conjugation, resulting in a pronounced nonlinear fluorescence quenching response to increasing guest concentration. This allosteric "turn-off" sensing mechanism enabled clear discrimination between benzenediols and simple phenols, since the sensing behavior is governed by both the number and position of the hydroxy groups and the resulting differences in molecular structure. These findings demonstrate that bisimidazole-based hydrindacene receptors function as highly tunable π-conjugated chromophores and show great promise as supramolecular fluorescent sensors.

Conflicts of interest

There are no conflicts to declare.

Data availability

The data supporting this article have been included as part of the supplementary information (SI). Supplementary information is available. See DOI: https://doi.org/10.1039/d5cp04027b.

CCDC 2325723 (**1a**)[35] and 2490135 (**2**)[54] contain the supplementary crystallographic data for this paper.

Acknowledgements

This work was supported by the JSPS KAKENHI (Grant Number JP17K19129, JP20K05478 and JP24K08385 for H. K.). The authors thank the Cooperative Research Program of "NJRC Mater. & Dev." from MEXT JAPAN.

Notes and references

1 Y. Yuan, J.-X. Chen, F. Lu, Q.-X. Tong, Q.-D. Yang, H.-W. Mo, T.-W. Ng, F.-L. Wong, Z.-Q. Guo, J. Ye, Z. Chen, X.-H. Zhang and C.-S. Lee, Bipolar Phenanthroimidazole Derivatives Containing Bulky Polyaromatic Hydrocarbons for Non-doped Blue Electroluminescence Devices with High Efficiency and Low Efficiency Roll-Off, *Chem. Mater.*, 2013, **25**, 4957–4965.

2 O. F. Al Sharif, L. M. Nhari, R. M. El-Shishtawy and A. M. Asiri, Imidazole-based fluorophores: synthesis and applications, *Mater. Today Chem.*, 2023, **29**, 101453.

3 W. Lin, L. Long, L. Yuan, Z. Cao, B. Chen and W. Tan, A Ratiometric Fluorescent Probe for Cysteine and Homocysteine Displaying a Large Emission Shift, *Org. Lett.*, 2008, **10**, 5577–5580.

4 A. D. Lama, J. P. Sestelo, L. Valencia, D. Esteban-Gómez, L. A. Sarandeses and M. M. Martínez, Synthesis and structural analysis of *push–pull* imidazole-triazole based fluorescent bifunctional chemosensor for Cu^{2+} and Fe^{2+} detection, *Dyes Pigm.*, 2022, **205**, 110539.

5 U. Krishnan, S. Manickam and S. K. Iyer, Turn-off fluorescence of imidazole-based sensor probe for mercury ions, *Sens. Diagn.*, 2024, **3**, 87–94.

6 Y. Zhang, S.-L. Lai, Q.-X. Tong, M.-F. Lo, T.-W. Ng, M.-Y. Chan, Z.-C. Wen, J. He, K.-S. Jeff, X.-L. Tang, W.-M. Liu, C.-C. Ko, P.-F. Wang and C.-S. Lee, High Efficiency Nondoped Deep-Blue Organic Light Emitting Devices Based on Imidazole-π-triphenylamine Derivatives, *Chem. Mater.*, 2012, **24**, 61–70.

7 W. Li, D. Liu, F. Shen, D. Ma, Z. Wang, T. Feng, Y. Xu, B. Yang and Y. Ma, A Twisting Donor-Acceptor Molecule with an Intercrossed Excited State for Highly Efficient, Deep-Blue Electroluminescence, *Adv. Funct. Mater.*, 2012, **22**, 2797–2803.

8 H. Huang, Y. Wang, S. Zhuang, X. Yang, L. Wang and C. Yang, Simple Phenanthroimidazole/Carbazole Hybrid Bipolar Host Materials for Highly Efficient Green and Yellow Phosphorescent Organic Light-Emitting Diodes, *J. Phys. Chem. C*, 2012, **116**, 19458–19466.

9 J. Kulhánek and F. Bureš, Imidazole as a parent π-conjugated backbone in charge-transfer chromophores, *Beilstein J. Org. Chem.*, 2012, **8**, 25–49.

10 W. Sun, N. Zhou, Y. Xiao, S. Wang and X. Li, A Novel Spiro[acridine-9,9′-fluorene] Derivatives Containing Phenanthroimidazole Moiety for Deep-Blue OLED Application, *Chem. – Asian J.*, 2017, **12**, 3069–3076.

11 Y. Li, Y. Li, Y. Zhao, T. Yu, W. Su, R. Wang, H. Ma and L. Qian, Investigation of the imidazole-derived moiety/spiro[fluorene-9,9′-xanthene] hybrid compounds for blue luminescent materials, *Synth. Met.*, 2021, **277**, 116771.

12 K. Sakai, S. Tsuchiya, T. Kikuchi and T. Akutagawa, An ESIPT fluorophore with a switchable intramolecular hydrogen bond for applications in solid-state fluorochromism and white light generation, *J. Mater. Chem. C*, 2016, **4**, 2011–2016.

13 S. Kothavale and N. Sekar, A New Series of Highly Fluorescent Blue-Green Emitting, Imidazole-Based ICT-ESIPT Compounds: Detail Experimental and DFT Study of Structural and Donating Group Effects on Fluorescence Properties, *ChemistrySelect*, 2017, **2**, 7691–7700.

14 K. P. Klubek, S.-C. Dong, L.-S. Liao, C. W. Tang and L. J. Rothberg, Investigating blue phosphorescent iridium cyclometalated dopant with phenyl-imidazole ligands, *Org. Electron.*, 2014, **15**, 3127–3136.

15 H. J. Park, E. A. Chae, H. W. Seo, J.-H. Jang, W. J. Chung, J. Y. Lee, D.-H. Hwang and U. C. Yoon, New blue phosphorescent heteroleptic Ir(III) complexes with imidazole- and *N*-methylimidazole carboxylates as ancillary ligands, *J. Mater. Chem. C*, 2020, **8**, 13843–13851.

16 J.-H. Kim, Y.-H. Jeong, H.-J. Yoon, H. Tran, L. M. Campos and W.-D. Jang, Cascade sensing of gold and thiols with imidazole-bearing functional porphyrins, *Chem. Commun.*, 2014, **50**, 11500–11503.

17 B. Kuzu, M. Tan, Z. Ekmekci and N. Menges, A novel fluorescent sensor based on imidazole derivative for Fe^{3+} ions, *J. Lumin.*, 2017, **192**, 1096–1103.

18 S. Sahu, Y. Sikdar, R. Bag, J. Cerezo, J. P. Cerón-Carrasco and S. Goswami, Turn on Fluorescence Sensing of Zn^{2+} Based on Fused Isoindole-Imidazole Scaffold, *Molecules*, 2022, **27**, 2859.

19 A. R. Nesaragi, P. Naik, B. B. A. Mulla, N. Al-Zaqri, C. C. Vidyasagar, N. K. Kalagatur, T. M. Sharanakumar, H. Guddappa, A. H. Sidarai and H. P. Shivarudrappa, Selective Al^{3+} and Fe^{3+} detection using imidazole–oxadiazole sensors: bioimaging evidence from zebrafish, *New J. Chem.*, 2025, **49**, 5729–5739.

20 J. R. Jadhav, C. H. Bae and H.-S. Kim, Fluorescence sensing of $H_2PO_4^-$ by a imidazolium-based cholestane receptor, *Tetrahedron*, 2011, **52**, 1623–1627.

21 H.-L. Ding, Y.-Q. Pu, D.-Y. Ye, Z.-Y. Dong, M. Yang, C.-W. Lü and Y. An, The design and synthesis of two imidazole fluorescent probes for the special recognition of HClO/$NaHSO_3$ and their applications, *Anal. Methods*, 2020, **12**, 2476–2483.

22 J. Kim, S. Lee, S. Kim, M. Jung, H. Lee and M. S. Han, Development of a fluorescent chemosensor for chloride ion detection in sweat using Ag^+-benzimidazole complexes, *Dyes Pigm.*, 2020, **177**, 108291.

23 Y. Wang, H. Liu, Z. Chen and S. Pu, Aggregation-induced emission enhancement (AIEE)-active tetraphenylethene (TPE)-based chemosensor for CN^-, *Spectrochim. Acta, Part A*, 2021, **245**, 118928.

24 X. Yu, Y. Li, Y. Li, Y. Liu and Y. Wang, A highly sensitive fluorescent sensor for reversible visual detection of fluoride ion and trace water in food products, *Spectrochim. Acta, Part A*, 2025, **326**, 125245.

25 S.-Y. Yin, S.-S. Sun, M. Pan, L. Chen, Z. Wang, Y.-J. Hou, Y.-N. Fan, H.-P. Wang and C.-Y. Su, An imidazole based ESIPT molecule for fluorescent detection of explosives, *J. Photochem. Photobiol., A*, 2018, **355**, 377–381.

26 Q. Hu, Q. Huang, K. Liang, Y. Wang, Y. Mao, Q. Yin and H. Wang, An AIE + TICT activated colorimetric and ratiometric fluorescent sensor for portable, rapid, and selective detection of phosgene, *Dyes Pigm.*, 2020, **176**, 108229.

27 (*a*) S. Zhang, Y. Huang, L. Kong, X. Zhang and J. Yang, Aggregation-induced emission-active tetraphenylethylene derivatives containing arylimidazole unit for reversible mechanofluorochromism and selective detection of picric acid, *Dyes Pigm.*, 2020, **181**, 108574; (*b*) Y. Yin, S. Zhang, X. He, X. Xu, G. Zhang, L. Yang, L. Kong and J. Yang, A novel tetraphenylethylene-functionalized arylimidazole AIEgen for detections of picric acid and Cu^{2+}, *Chem. Pap.*, 2021, **75**, 6297–6306.

28 S. Yi, H. Liu, Z. Chen, C. Fan, G. Liu and S. Pu, Novel fluorescent probes based on NBD-substituted imidazole amino to sequentially detect H_2S and Zn^{2+}, *Dyes Pigm.*, 2023, **214**, 111211.

29 M. M. Zafar, S. C. Sahoo, V. K. Praveen, N. Tyagi and R. K. Mishra, Imidazole-assisted film-based fluorescent sensor for the ultrasensitive detection of hydrazine, *J. Mater. Chem. C*, 2024, **12**, 7472–7481.

30 Y. Ma, L. Zhang, H. Yang, S. Zhu and J. Liu, Imidazole-triggered *in situ* fluorescence reaction system for quantitatively determination of dopamine from multiple sources, *Talanta*, 2025, **292**, 127975.

31 S. Shinkai, M. Ikeda, A. Sugasaki and M. Takeuchi, Positive Allosteric Systems Designed on Dynamic Supramolecular Scaffolds: Toward Switching and Amplification of Guest Affinity and Selectivity, *Acc. Chem. Res.*, 2001, **34**, 494–503.

32 A. F. Rodríguez-Serrano and I.-M. Hsing, Allosteric Regulation of DNA Circuits Enables Minimal and Rapid Biosensors of Small Molecules, *ACS Synth. Biol.*, 2021, **10**, 371–378.

33 N. Yu, C. Zhao, X. Kang, C. Zhang, X. Zhang, C. Li, S. Wang, B. Xue, X. Yang, C. Li, Z. Qiu, J. Wang and Z. Shen, Ultrasensitive Electrochemical Biosensors Based on Allosteric Transcription Factors (aTFs) for Pb^{2+} Detection, *Biosensors*, 2024, **14**, 446.

34 Q. Zhang, Z. Wei and X. Jia, Controllable detection threshold achieved through the toehold switch system in a mercury ion whole-cell biosensor, *Biosens. Bioelectron.*, 2024, **256**, 116283.

35 T. Kataoka, K. Matsumura, K. Ono, Y. Tsuchido and H. Kawai, Aromatic Ring-Fused Amidine Based Allosteric Receptors Activated by Guest-Induced π-Conjugation Switching, *ChemPlusChem*, 2025, **90**, e202400612.

36 F. Dierschke and K. Müllen, Blue Emission of a Soluble Poly(*p*-phenylene) with a Cross-Conjugated Bisimidazole-Based Chromophore, *Macromol. Chem. Phys.*, 2007, **208**, 37–43.

37 L. Zhang and F. Liu, Synthesis of Bisimidazole Derivatives for Selective Sensing of Fluoride Ion, *Molecules*, 2017, **22**, 1519.

38 X.-T. Kan, H. Yao, Y.-B. Niu, Y.-P. Hu, Y.-M. Zhang, T.-B. Wei and Q. Lin, Regulation of conjugate rigid plane structures for achieving transformation of fluorescence recognition properties, *New J. Chem.*, 2022, **46**, 2858–2862.

39 P. J. Goutam and P. K. Iyer, Selective detection of resorcinol using a bis(benzothiazol-2-yl)pyridine based ditopic receptor, *Sens. Actuators, B*, 2015, **211**, 263–267.

40 W. Ren, Y. Zhang, W. Y. Liang, X. P. Yang, W. D. Jiang, X. H. Liu and W. Zhang, A facile and sensitive ratiometric fluorescence sensor for rapid visual monitoring of trace resorcinol, *Sens. Actuators, B*, 2021, **330**, 129390.

41 T. Long, J. Cheng, C. Peng, W. Xu, H. Luo, M. Ouyang, D. Xu, Q. Lin, J. Qu and X. Huang, Highly sensitive and rapid detection of resorcinol by forming fluorescent azamonardine with dopamine, *Anal. Biochem.*, 2022, **642**, 114562.

42 X.-J. Wang, Y. Xu, L. Zhang, D. Krishnamurthy and C. H. Senanayake, Mild Iodine−Magnesium Exchange of Iodoaromatics Bearing a Pyrimidine Ring with Isopropylmagnesium Chloride, *Org. Lett.*, 2006, **8**, 3141–3144.

43 F. Zapata, A. Caballero, A. Espinosa, A. Tárraga and P. Molina, Imidazole-Annelated Ferrocene Derivatives as Highly Selective and Sensitive Multichannel Chemical Probes for Pb(II) Cations, *J. Org. Chem.*, 2009, **74**, 4787–4796.

44 H. Kawai, R. Katoono, K. Nishimura, S. Matsuda, K. Fujiwara, T. Tsuji and T. Suzuki, Positive Homotropic Allosteric Binding of Benzenediols in a Hydrindacene-Based Exoditopic Receptor: Cooperativity in Amide Hydrogen Bonding, *J. Am. Chem. Soc.*, 2004, **126**, 5034–5035.

45 We excluded hydroquinone from the investigation due to its significantly low solubility under the experimental conditions and previous results indicating no binding with the diamide receptor.

46 (*a*) D. B. Hibbert and P. Thordarson, The death of the Job plot, transparency, open science and online tools, uncertainty estimation methods and other developments in supramolecular chemistry data analysis, *Chem. Commun.*, 2016, **52**, 12792–12805; (*b*) BindFit, https://supramolecular.org.

47 The binding constant of phenol could not be estimated due to its small shift.

48 C. Hansch, A. Leo and R. W. Taft, A survey of Hammett substituent constants and resonance and field parameters, *Chem. Rev.*, 1991, **91**, 165–195.

49 The fluorescence quenching observed for receptor **2** presumably arises from the protonation of the naphthoimidazole units by TFA, which lowers their electron-donating capability and inhibits the emission process based on intramolecular charge transfer (ICT).

50 The absorption bands of **1a** and **1b** overlapped with those of the benzenediols, which prevented the accurate determination of their λ_{abs} shifts.

51 K. Feng, F.-L. Hsu, D. V. DerVeer, K. Bota and X. R. Bu, Tuning fluorescence properties of imidazole derivatives with thiophene and thiazole, *J. Photochem. Photobiol., A*, 2004, **165**, 223–228.

52 E. Ciotta, P. Prosposito and R. Pizzoferrato, Positive curvature in Stern-Volmer plot described by a generalized model for static quenching, *J. Lumin.*, 2019, **206**, 518–522.

53 M. H. Gehlen, The centenary of the Stern–Volmer equation of fluorescence quenching: from the single line plot to the SV quenching map, *J. Photochem. Photobiol., C*, 2020, **42**, 100338.

54 CCDC 2490135: Experimental Crystal Structure Determination, 2026, DOI: 10.5517/ccdc.csd.cc2pl5yf.

